ARTICLE OPEN

Check for updates

A $j_{\mathrm{eff}} = 1/2$ Kitaev material on the triangular lattice: the case of $NaRuO_2$

Aleksandar Razpopov[1]✉, David A. S. Kaib[1]✉, Steffen Backes[2,3,4], Leon Balents[5], Stephen D. Wilson[6], Francesco Ferrari[1], Kira Riedl[1] and Roser Valentí[1]✉

Motivated by recent reports of a quantum-disordered ground state in the triangular lattice compound $NaRuO_2$, we derive a $j_{\mathrm{eff}} = 1/2$ magnetic model for this system by means of first-principles calculations. The pseudospin Hamiltonian is dominated by bond-dependent off-diagonal Γ interactions, complemented by a ferromagnetic Heisenberg exchange and a notably antiferromagnetic Kitaev term. In addition to bilinear interactions, we find a sizable four-spin ring exchange contribution with a strongly anisotropic character, which has been so far overlooked when modeling Kitaev materials. The analysis of the magnetic model, based on the minimization of the classical energy and exact diagonalization of the quantum Hamiltonian, points toward the existence of a rather robust easy-plane ferromagnetic order, which cannot be easily destabilized by physically relevant perturbations.

npj Quantum Materials (2023)8:36; https://doi.org/10.1038/s41535-023-00567-6

INTRODUCTION

The first definition of a quantum spin liquid (QSL) state dates back to the milestone paper by P.W. Anderson in 1973[1], in which the *resonating valence-bond* wave function, a macroscopic liquid-like superposition of singlet states, was proposed as a variational guess for the ground state of the triangular lattice Heisenberg antiferromagnet[2,3]. Another archetypal portrait of a QSL state is more recent and originated from the seminal work of Kitaev[4], who set a bond-anisotropic spin model on the honeycomb lattice with an exact spin-liquid ground state represented in terms of Majorana fermions. Both these alternative descriptions of QSL states, which are associated with different microscopic mechanisms of frustration, left an indelible mark in the context of frustrated magnetism. On the one hand, the triangular lattice antiferromagnet is the prototypical example of a system with *geometric frustration*, where the presence of antiferromagnetic Heisenberg couplings over odd-sided loops of sites fights the tendency toward long-range magnetic order. On the other hand, the possibility of realizing *anisotropic interactions* as a consequence of the interplay between spin–orbit coupling (SOC), crystal field splitting and Hund's coupling[5–7] has opened a whole new field of investigation centered around the Kitaev materials[8–10]. Even though the original Kitaev honeycomb model has no odd-sided loops and hence no geometric frustration, it nevertheless features *exchange frustration*[10,11] due to the fact that bond-directional interactions with competing quantization axes cannot be satisfied simultaneously.

In this work, we investigate a recently synthesized compound, $NaRuO_2$, in which both paradigms of magnetic frustration described above come into play. The crystal structure of this material displays perfect triangular lattice planes of edge-sharing RuO_6 octahedra, separated by Na ions[12–14] (illustrated in Fig. 1). The space group of $NaRuO_2$ is $R\bar{3}m$. The same structural arrangement is found in a family of rare-earth chalcogenides which have been recently investigated as possible spin liquid candidates[15]: $NaYbO_2$[16], $NaYbS_2$[17,18], and $NaYbSe_2$[19]. However, at variance with the latter, in $NaRuO_2$ the rare-earth ion is replaced by ruthenium, which belongs to the *d*-block of the periodic table. In analogy to the intensively studied honeycomb compound α-$RuCl_3$[8–10], the strong SOC of ruthenium, combined with the geometry of edge-sharing ligand octahedra, is expected to realize a prime example for the Jackeli–Khaliullin mechanism to form a $j_{\mathrm{eff}} = 1/2$ magnet with significant Kitaev interaction[7]. Resistivity measurements identified $NaRuO_2$ to be indeed insulating, with a small magnetization upon application of an external magnetic field, and a paramagnetic Curie temperature dependence of the magnetic susceptiblity[13]. These signatures point toward the possibility of a QSL ground state, making a microscopically motivated magnetic model for $NaRuO_2$ not only intriguing but also necessary.

The interplay between Heisenberg exchange and Kitaev interactions on the triangular lattice[20,21] has been investigated in several works, revealing, for instance, the presence of crystals of $\mathbb{Z}_2$ vortices in the proximity of the magnetic phase with 120° order[22], and possibly a spin nematic state around the antiferromagnetic Kitaev point[23–25]. Furthermore, an extended spin model featuring the Γ-exchange coupling[26], which can favor the onset of a stripy magnetic phase, has been investigated in connection with the $j_{\mathrm{eff}} = 1/2$ iridate compound $Ba_3IrTi_2O_9$[27,28]. In this regard, a comprehensive overview of the different phases induced by bond-anisotropic (nearest-neighbor) couplings on the triangular lattice is provided by ref. [29]. More recently, analogous anisotropic spin Hamiltonians have been shown to capture the effective magnetic interactions of certain transition metal dihalides[30–32].

In addition to bilinear spin couplings, several magnetic materials with a triangular lattice structure, e.g., organic charge-transfer salts[33], are characterized by non-negligible four-spin ring exchange interactions[34], which incorporate higher-order contributions in the perturbation-theory treatment of the Hubbard model around the Mott insulating regime. While at the (semi-)classical level ring exchange can induce the formation of spirals and

[1]Institut für Theoretische Physik, Goethe-Universität, 60438 Frankfurt am Main, Germany. [2]Research Center for Advanced Science and Technology, University of Tokyo, Komaba, Tokyo 153-8904, Japan. [3]Center for Emergent Matter Science, RIKEN, Wako, Saitama 351-0198, Japan. [4]CPHT, CNRS, École polytechnique, Institut Polytechnique de Paris, 91120 Palaiseau, France. [5]Kavli Institute for Theoretical Physics, University of California, Santa Barbara, CA 93106, USA. [6]Materials Department, University of California, Santa Barbara, CA, USA. ✉email: razpopov@itp.uni-frankfurt.de; kaib@itp.uni-frankfurt.de; valenti@itp.uni-frankfurt.de

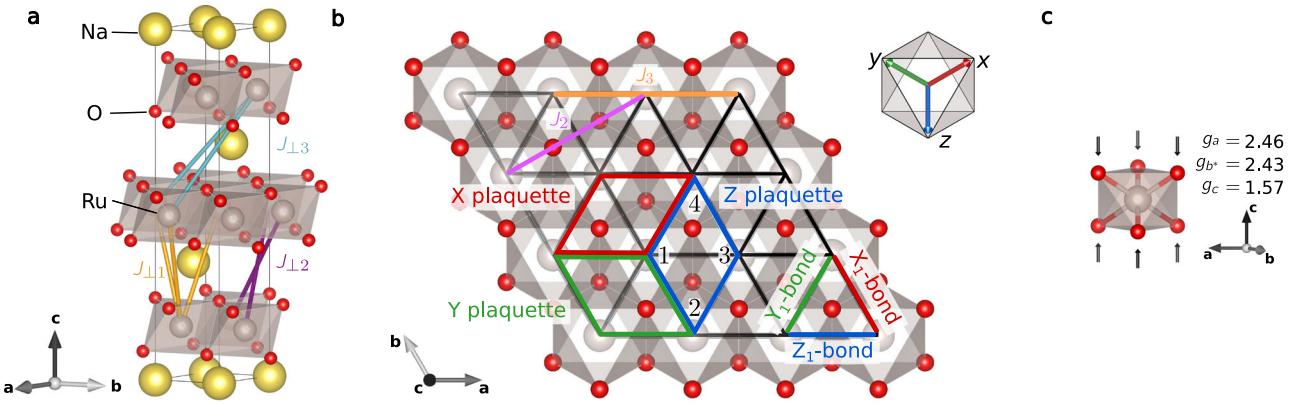

Fig. 1 $NaRuO_2$ crystal structure, illustrations, and DFT results for the *g*-tensor values. a Crystal structure of $NaRuO_2$ with an illustration of interlayer bonds $J_{\perp i}$. **b** Top view of the triangular Ru lattice, with an illustration of intralayer bonds and four-spin ring exchange plaquettes. The cubic coordinates employed in the magnetic model are oriented approximately along Ru–O bonds, as shown in the top right corner. **c** Trigonally compressed RuO_6 octahedron and corresponding ab-initio *g*-tensor values, with b^* defined perpendicular to the crystallographic *a* and *c* axes.

non-trivial chiral orders (e.g., spin-vortex crystals)[35], or significantly affect the low-energy magnon spectra of collinear phases[36], at the quantum level it is argued to potentially stabilize QSL phases[37,38]; in this regard, the possible appearance of a gapless QSL with a spinon Fermi surface[39], or a Kalmeyer–Laughlin chiral state[40], has been discussed. An additional level of complication arises in magnetic systems with strong spin–orbit interactions, namely the presence of spin-anisotropic ring-exchange interactions, which have been scarcely investigated in the past[41].

In this work, we perform a thorough inspection of the magnetic properties of $NaRuO_2$, from first-principles calculations to microscopic spin models. We provide theoretical justification for the low-energy description of $NaRuO_2$ in terms of $j_{\text{eff}} = 1/2$ pseudospin degrees of freedom, highlighting the importance of different sources of interactions, such as intra- and inter-layer exchange couplings, and bond-anisotropic bilinear and ring-exchange interactions stemming from the strong SOC effects. The analysis of (classical and quantum) magnetic models indicate the existence of a robust easy-plane ferromagnetic (FM) order, which cannot be easily destabilized by perturbations around the ab initio derived spin Hamiltonian. Based on our proposed magnetic model, we also provide theoretical inelastic neutron scattering (INS) spectra, which can be directly compared to the experiment.

ELECTRONIC PROPERTIES

We begin by analyzing the electronic properties of $NaRuO_2$ with the help of density functional theory (DFT) calculations, as detailed in the "Methods" section. The octahedral environment of the Ru $4d^5$ sites leads to a crystal field splitting[8,42,43] with unoccupied e_g-states and occupied t_{2g}-states. The latter further split into $j_{\text{eff}} = 3/2$ and $j_{\text{eff}} = 1/2$ levels in the limit of strong SOC.

To estimate the Hubbard repulsion and Hund's coupling of $NaRuO_2$, we employ constrained random phase approximation (cRPA) calculations (see "Methods" section). In the non-relativistic band structure, we observe a crossing between the Ru e_g band and a band with dominant Na 3*s* character close to the Γ point. This poses the question of which bands should be included in the Wannierization procedure prior to cRPA. One option is considering only the five 4*d* Ru bands, which can be expected to lead to an artificially enhanced e_g screening. The corresponding cRPA result is $(U_{\text{avg}}, J_{\text{avg}})_{4d} = (3.114, 0.4736)$ eV. Alternatively, the crossing band may be included in a cRPA calculation based on a six-band model. This choice leads to an artificially suppressed screening, with $(U_{\text{avg}}, J_{\text{avg}})_{4d+3s} = (3.1865, 0.4756)$ eV. Since it turns out that

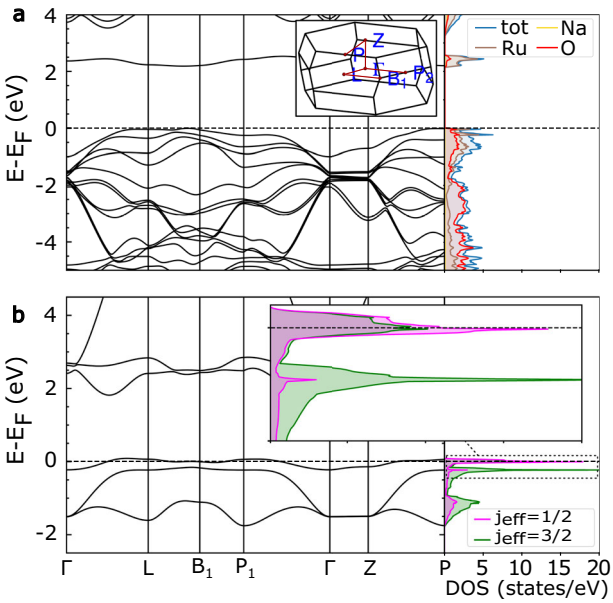

Fig. 2 Electronic band structure and density of states of $NaRuO_2$. **a** Ferromagnetic GGA+SOC+U results, with $(U_{\text{avg}}, J_{\text{avg}}) = (3.15, 0.47)$ eV for the Ru 4*d* electrons, and magnetization polarized in the crystallographic *a*–*b* plane. **b** Non-magnetic GGA + SOC results. The partial DOS for Ru 4*d* orbitals projected in the j_{eff} basis (see Supplementary Note 1) shows a dominant $j_{\text{eff}} = 1/2$ weight close to the Fermi energy (see inset).

both approaches lead to similar results, we choose to work with the average of them: $(U_{\text{avg}}, J_{\text{avg}}) = (3.15, 0.47)$ eV.

We employ these values as correlation corrections on the Ru 4*d* electrons in a relativistic band structure calculation (GGA + SOC + U, see "Methods" section) with ferromagnetically aligned magnetic moments. The resulting band structure and partial DOS are shown in Fig. 2a. We choose the spin magnetic moments to be polarized in the crystallographic *a*–*b* plane, which is the most energetically favorable orientation. Within this setting, we obtain an insulator with a charge gap of 2.1 eV which is in agreement with recent resistivity experiments[13]. We find that the combination of magnetism and Coulomb interaction is necessary to open a realistic charge gap in $NaRuO_2$, which is further enlarged by SOC.

The partial DOS resolves the dominance of ruthenium weight around the Fermi level, such that we can proceed with low-energy modeling of this compound based on ruthenium bands.

The edge-sharing octahedral structure of $NaRuO_2$ hints towards the possibility of a $j_{\text{eff}} = 1/2$ description of the low-energy magnetic properties, in analogy with the intensively studied α-$RuCl_3$[8]. To check the validity of the $j_{\text{eff}} = 1/2$ picture for $NaRuO_2$, we calculate the non-magnetic band structure and project the DOS in the $j_{\text{eff}} = \{1/2, 3/2\}$ basis obtained by considering only t_{2g} orbitals (see Supplementary Note 1). The results, reported in Fig. 2b, show that the character of the DOS around the Fermi energy is dominated by $j_{\text{eff}} = 1/2$ states, thus justifying a low-energy description in terms of $j_{\text{eff}} = 1/2$ pseudospins.

Magnetic model

As an appropriate magnetic model for $NaRuO_2$, we consider a $j_{\text{eff}} = 1/2$ pseudospin Hamiltonian. To relate the pseudospin $\mathbf{S}$ of the magnetic Hamiltonian to the magnetic moment, $\mathbf{M} = \mu_B \mathbb{G} \cdot \mathbf{S}$, we calculate the gyromagnetic g-tensor from first principles (see "Methods" section). We find it to be approximately diagonal with $(g_a, g_{b^*}, g_c) = (2.46, 2.43, 1.57)$ in crystallographic coordinates (with b^* perpendicular to a and c). With respect to the triangular plane, the in-plane components (g_a, g_{b^*}) are larger than the out-of-plane one (g_c), as a direct consequence of the trigonal compression of the RuO_6 octahedra along the crystallographic c axis (see Fig. 1c)[44].

For the magnetic interactions between the pseudospins, we consider a Hamiltonian consisting of a bilinear exchange term $\mathcal{H}_2$ and a four-spin ring exchange term $\mathcal{H}_4$. We express this model in the conventionally used cubic coordinates for Kitaev materials, which consist of orthogonalized axes oriented approximately along the Ru-O bonds, as illustrated in the top right corner of Fig. 1b. We denote the three components of the pseudospin at site i as S_i^μ, with $\mu = \{x, y, z\}$. In this framework, the [111] pseudospin direction is parallel to the crystallographic c-axis. For completion, in Supplementary Note 2 we translate our model to an alternative reference frame with crystallographic coordinates[29].

The bilinear contribution to the magnetic Hamiltonian $\mathcal{H}_2 = \sum_{i<j} \sum_{\mu\nu} \mathbb{J}_{ij}^{\mu\nu} S_i^\mu S_j^\nu$ contains, especially for nearest neighbors, anisotropic bond-dependent terms. Considering the symmetry constraints of the $R\bar{3}m$ space group, the bilinear exchange tensor on a Z_1-bond (as defined in Fig. 1b) follows the form

$$\mathbb{J}_{Z_1\text{-bond}} = \begin{pmatrix} J_1 & \Gamma_1 & \Gamma_1' \\ \Gamma_1 & J_1 & \Gamma_1' \\ \Gamma_1' & \Gamma_1' & J_1 + K_1 \end{pmatrix}. \quad (1)$$

Here, J_1 is the isotropic Heisenberg exchange, K_1 is the Kitaev coupling, and Γ_1 and Γ_1' the off-diagonal symmetric exchange parameters. The bilinear interactions on X_1- and Y_1-bonds are then related to this expression by C_3 spin rotations around the [111] axis, amounting to cyclic permutation of (x, y, z) spin components.

We performed DFT calculations to obtain the magnetic exchange parameters as described in the "Methods" section. In Table 1 we show the dominant magnetic couplings extracted for nearest-neighbor bonds with the projED method[45] and the isotropic longer-range exchange from total energy mapping analysis (TEMA). Both methods predict a dominant intralayer FM Heisenberg J_1 coupling. However, for a quantitative agreement of the results, larger U values in the DFT + U calculations with respect to projED should be considered in this case. This is to be expected since the two techniques rely on different implementations of the Coulomb terms (see "Methods"). The readjustment can be directly taken into account by considering a scaling factor $J_1^{\text{projED}}/J_1^{\text{TEMA}} \approx 0.65$ for the Heisenberg exchange couplings obtained by TEMA. This is justified by the fact that the ratio between different Heisenberg exchange couplings does not vary significantly as a function of U for this system. In addition to the strong nearest-neighbor FM J_1, the shortest further-neighbor intralayer exchange couplings are found to be non-negligible and of similar magnitude, with J_2 being anti- and J_3 ferromagnetic. The interlayer Heisenberg couplings $J_{\perp 1}$, $J_{\perp 2}$, and $J_{\perp 3}$ (shown in Fig. 1a) are one magnitude smaller than the intralayer ones, with $J_{\perp 1}$ and $J_{\perp 2}$ being ferromagnetic and $J_{\perp 3}$ antiferromagnetic.

Table 1. Magnetic exchange parameters.

	d_{Ru-Ru} [Å]	$\mathcal{J}$ [meV]
J_1	3.056	−4.16
K_1		+2.86
Γ_1		+7.00
Γ_1'		+0.65
J_2	5.293	+1.86
J_3	6.112	−1.64
$J_{\perp 1}$	5.656	−0.14
$J_{\perp 2}$	6.429	−0.73
$J_{\perp 3}$	7.118	+0.39

Calculated magnetic interactions ($\mathbb{J}_1$ matrix, see Eq. (1)) for the nearest neighbor, and the longer-range intra- (J_i) and interlayer ($J_{\perp i}$) bonds. The nearest neighbor couplings, as defined in Eq. (1), are extracted with the projED method, while the isotropic J couplings are determined by TEMA within the VASP framework. The TEMA results are scaled by a factor of $J_1^{\text{projED}}/J_1^{\text{TEMA}} = 0.65$ (see main text).

Within the projED method, we obtain the bond-dependent anisotropic couplings K_1, Γ_1, and Γ_1' at nearest-neighbors, where the cRPA values $(U_{\text{avg}}, J_{\text{avg}}) = (3.15, 0.47)$ eV are employed. Compared to previously estimated magnetic parameters for other Ru $4d$ systems[46–49], it is interesting to note that we have strongly *antiferromagnetic* Kitaev K_1 term and a dominant positive Γ_1 as the largest coupling. These are contributions that, to the best of our knowledge, have not been observed in a real material with effective spin 1/2 so far.

The microscopic origin of the unusual antiferromagnetic sign of the Kitaev interaction encountered here can be understood as follows: from the perspective of second-order perturbation theory in a perfect octahedral environment (considering only the occupied t_{2g} orbitals)[50], the Kitaev interaction scales as $K_1 \propto (t_1 - t_3)^2 - 3t_2^2$. On a Z-bond, the hopping parameters are defined as the ligand-assisted hopping $t_2 = t_{(xz;yz)}$, as well as $t_1 = t_{(xz;xz)} = t_{(yz;yz)}$ and $t_3 = t_{(xy;xy)}$, which stem predominantly from direct d orbital overlap. For the prime example of the honeycomb Kitaev material α-$RuCl_3$, the indirect hopping t_2 is dominant, somewhat close to the t_2-only model in the Jackeli-Khaliullin mechanism, where the Kitaev interaction is FM ($K_1 \propto -3t_2^2$)[7]. In comparison, the direct hoppings t_3 and t_1 gain importance in $NaRuO_2$, where the nearest neighbor Ru-Ru bond length is significantly smaller than in α-$RuCl_3$. Indeed, for $NaRuO_2$, a non-relativistic DFT calculation yields $t_1 = 80$ meV, $t_2 = 125$ meV and $t_3 = -261$ meV. As dictated by the geometry, t_3 is negative and larger in magnitude than the positive t_1. The resulting *antiferromagnetic* Kitaev interaction in $NaRuO_2$ can hence be directly related to the shorter nearest-neighbor bond length of this triangular compound. The perturbation theory perspective also offers an explanation for the dominance of the off-diagonal symmetric exchange Γ_1, which scales approximately as $\Gamma_1 \propto t_2(t_1 - t_3)$[50]. While the magnitude of K_1 reduces with the competition between indirect and direct contributions, Γ_1 increases proportional to the magnitude of the hoppings, leading to a magnetic model dominated by the off-diagonal symmetric exchange for $NaRuO_2$.

Despite the antiferromagnetic sign of the Kitaev interaction, the bilinear exchange Hamiltonian $\mathcal{H}_2$ features a ferromagnetically

ordered ground state, due to significant $J_1 < 0$ and $\Gamma_1 > 0$ interactions, as discussed in more detail below. To seek out possible additional interactions that might destabilize the FM ground state, we consider the effects of higher-order ring exchange interactions. Compared to honeycomb Kitaev materials, $NaRuO_2$ could be predestined for such interactions, due to the marginally insulating Mott state reported in experiments[13] and to its triangular lattice structure, where the shortest closed loops consist of four (instead of six) sites. Four-spin ring exchange without SOC effects has been discussed plentifully in the literature[34,36–38,40] and takes the form

$$\mathcal{H}_4^{\mathrm{iso}} = \frac{K^{\mathrm{iso}}}{S^2} \sum_{\langle ijkl \rangle} (\mathbf{S}_i \cdot \mathbf{S}_j)(\mathbf{S}_k \cdot \mathbf{S}_l) + (\mathbf{S}_i \cdot \mathbf{S}_l)(\mathbf{S}_j \cdot \mathbf{S}_k) - (\mathbf{S}_i \cdot \mathbf{S}_k)(\mathbf{S}_j \cdot \mathbf{S}_l), \tag{2}$$

where the summation $\langle ijkl \rangle$ goes over plaquettes with sites i and k lying across a diagonal[34], K^{iso} is the coupling constant, and the superscript "iso" denotes that this is the conventional isotropic (i.e., SU(2)-symmetric) ring exchange. Note that the prefactor conventions for the ring exchange interaction vary in the literature[35,39,40,51]. Here, we choose to include a factor $\frac{1}{S^2}$ in Eqs. (2), (3). Thus, in the convention without this prefactor (e.g., ref. [40]), the ring exchange coupling constants we compute below would appear four times larger.

However, for $NaRuO_2$ there is no reason why the ring exchange between the pseudospin $j_{\mathrm{eff}} = \frac{1}{2}$ moments should follow the form of $\mathcal{H}_4^{\mathrm{iso}}$, since SOC is expected to induce anisotropic four-site terms in the Hamiltonian. In the most general form, an anisotropic four-spin exchange may be expressed as

$$\mathcal{H}_4^{\mathrm{tot}} = \frac{1}{S^2} \sum_{\langle ijkl \rangle} \sum_{\mu\nu\rho\eta} \mathbb{K}_{ijkl}^{\mu\nu\rho\eta} \left(S_i^\mu S_j^\nu S_k^\rho S_l^\eta\right), \tag{3}$$

where the tensor $\mathbb{K}$ contains the coupling constants. The presence of inversion symmetry with respect to the center of each plaquette, together with a C_2 rotation axis parallel to the shortest diagonal, reduces the 81 entries of $\mathbb{K}$ for one plaquette to 24 independent parameters. Furthermore, analogous to the X-, Y-, and Z-bonds of bilinear exchange, it is convenient to define X-, Y-, and Z-plaquettes, as shown in Fig. 1b. The three plaquettes are related by C_3 rotations around the out-of-plane axis and hence the tensor of one plaquette type fully encodes $\mathcal{H}_4^{\mathrm{tot}}$.

Note that in contrast to conventional ring exchange, care has to be taken for the order of the site numbering within a plaquette. For example, for a single plaquette (with the site labeling illustrated in Fig. 1b), swapping two sites across a diagonal is not a symmetry of the ring-exchange tensor, i.e., $\mathbb{K}_{1234}^{\mu\nu\rho\eta} \neq \mathbb{K}_{1432}^{\mu\nu\rho\eta}$, even in presence of the aforementioned symmetries.

To compute the ring-exchange tensor $\mathbb{K}$ from first principles, we employ the projED method, which has been used previously to determine ring-exchange couplings for organic triangular lattice compounds[35,52]. Results on a Z-plaquette are given in Table 2, and details of the calculation are outlined in the "Methods" section. We do not attempt to create a minimal model here and show agnostically the full ab-initio result. Overall, the four-site ring exchange contribution in $NaRuO_2$ does not seem to be obviously negligible, with a strength of roughly 5–10% of the nearest-neighbor bilinear exchange parameters. As anticipated, the shown results deviate substantially from the conventional isotropic ring exchange $\mathcal{H}_4^{\mathrm{iso}}$. This is not surprising because of the strong SOC in $NaRuO_2$. For instance, among the diagonal components characterizing the Z-plaquette, the $\mathbb{K}_{1234}^{zzzz}$ term strongly differs from $\mathbb{K}_{1234}^{xxxx} = \mathbb{K}_{1234}^{yyyy}$.

To quantify the degree of anisotropy of the total ring exchange Hamiltonian encoded in Table 2, we express it as a sum consisting of the conventional isotropic ring exchange from Eq. (2) and a purely anisotropic contribution: $\mathbb{K}^{\mathrm{tot}} = \mathbb{K}^{\mathrm{iso}} + \mathbb{K}^{\mathrm{ani}}$. The choice of this splitting is not unique, but we choose the coupling constant

Table 2. Four-spin ring exchange couplings for $NaRuO_2$.

$\mathbb{K}_{1234}^{\mu\nu\rho\eta}$ [meV]	$S_1^\mu S_2^\nu S_3^\rho S_4^\eta$
0.1829	(xxzx + yyzy + zxxx + zyyy)
0.1828	(xxzy + yxzy + zyxx + zyyx)
0.1819	(zxzy + zyzx)
0.1810	(xzyz + yzxz)
−0.1740	(zzzz)
−0.1559	(xyzz + yzzx + zxyz + zzxy)
−0.1457	(xzzx + yyzz + zxxz + zzyy)
−0.1398	(xxxx + yyyy)
−0.1284	(xxxz + xzxx + yyyz + yzyy)
0.1122	(zxzz + zyzz + zzzx + zzzy)
−0.0969	(xyxy + yxyx)
−0.0829	(xyzy + yxzx + zxyx + zyxy)
0.0602	(xyzx + yyzx + zxxy + zxyy)
−0.0596	(xyxz + xzxy + yxyz + yzyx)
−0.0581	(xzzz + yzzz + zzxz + zzyz)
−0.0580	(xxzz + yzzy + zyyz + zzxx)
−0.0570	(xzyx + xzyy + yxxz + yyxz)
−0.0542	(xxxy + xyxx + yxyy + yyyx)
0.0354	(xxyz + xyyz + yzxx + yzxy)
−0.0352	(xzzy + yxzz + zyxz + zzyx)
−0.0272	(xxyy + xyyx + yxxy + yyxx)
0.0252	(xzxz + yzyz)
0.0145	(xxyx + xyyy + yxxx + yyxy)
0.0069	(zxzx + zyzy)

The corresponding ring-exchange expression is defined in Eq. (3) and the parameters in this table refer to a Z-plaquette, with the site labeling 1, 2, 3, 4 illustrated in Fig. 1b. The ring-exchange parameters are calculated with projED starting from a three-orbital Hubbard model. For simplicity, we abbreviate $S_1^\mu S_2^\nu S_3^\rho S_4^\eta$ with "$\mu\nu\rho\eta$". Parameters for X- and Y-plaquettes follow by C_3 rotations around the out-of-plane axis.

K^{iso} in $\left(\mathbb{K}^{\mathrm{iso}}\right)_{1234}^{\mu\nu\rho\eta} = K^{\mathrm{iso}}\left(\delta_{\mu\nu}\delta_{\rho\eta} + \delta_{\mu\eta}\delta_{\nu\rho} - \delta_{\mu\rho}\delta_{\nu\eta}\right)$ (cf. Eq. (2)) such that the tensor-norm of the anisotropic part, $\|\mathbb{K}^{\mathrm{ani}}\| = \|\mathbb{K}^{\mathrm{tot}} - \mathbb{K}^{\mathrm{iso}}\|$, is minimized. Here, the tensor 1-norm is used ($\|\mathbb{K}\| = \sum_{\mu\nu\rho\eta} |\mathbb{K}_{1234}^{\mu\nu\rho\eta}|$). This choice is motivated by an analogy to the case of the bilinear Hamiltonian, where the same procedure splits the bilinear exchange tensor $\mathbb{J}_{ij}^{\mu\nu}$ into an (isotropic) Heisenberg exchange part and an anisotropic part, arriving at the same definition of Heisenberg-J as in Eq. (1). Dissecting the ring-exchange interaction in this way leads to $K^{\mathrm{iso}} = -0.06$ meV and $\|\mathbb{K}^{\mathrm{ani}}\| / \|\mathbb{K}^{\mathrm{iso}}\| = 5.6$, which shows that ring exchange in $NaRuO_2$ is dominated by the anisotropic contributions.

Properties of the magnetic model

We investigate the ground state of the magnetic model given in Table 1 by applying two different methods. We consider the classical ground state via an iterative minimization method of the energy[53,54] and then we include quantum fluctuations by tackling the Hamiltonian with exact diagonalization (ED) on finite clusters with up to 27 sites (see "Methods" section and Supplementary Note 3).

First, we consider the classical ground state of the $\mathcal{H}_2$ Hamiltonian restricted to the triangular lattice plane. The omission of inter-layer couplings is justified by their small estimated magnitude compared to intra-layer couplings (cf. Table 1). The

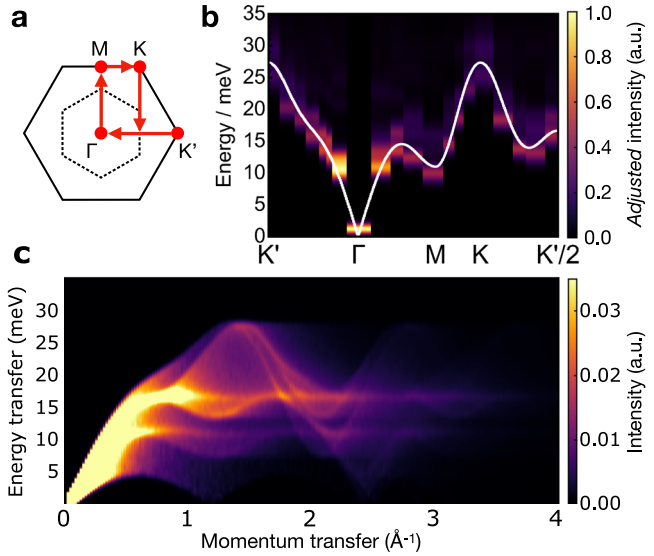

Fig. 3 Computed neutron scattering intensity within the magnetic model. a Momentum path in the Brillouin zone of the triangular lattice, **b** INS intensity for the Hamiltonian $\mathcal{H}_2$ without inter-plane interaction along the high symmetry lines in momentum space. The color plot shows ED results combined from different clusters up to 27 sites. Due to elsewise overbearing intensity at $\mathbf{q} = 0$, the plotted intensity is *adjusted* for $\mathbf{q} = 0$, by reducing the plotted intensity and broadening at $\mathbf{q} = 0$ (see "Methods"). The overlayed band dispersion is the single-magnon energy from LSWT. As the ED ground state is a superposition of different degenerate magnetic domains, the compared LSWT energy is plotted as the average of three calculations, corresponding to expansions around in-plane ferromagnetic order, with polarization perpendicular to X_1-, Y_1- or Z_1-bonds. **c** Calculated powder-averaged INS spectrum from LSWT, for the model in Table 1, including inter-plane exchange couplings. Intensities above ~3.5% of the maximum intensity are cut off due to large intensity at $\mathbf{q} \approx 0$.

minimum of the classical energy is provided by an FM spin arrangement, with spins lying in the triangular lattice plane. The FM nature of the ground state turns out to be stable upon different perturbations of the Hamiltonian around the ab initio model (as discussed in Supplementary Note 4) and upon the inclusion of anisotropic ring exchange or out-of-plane interactions. For what concerns the latter, the classical energy minimum yields an FM ground state, with spins being parallel to each other both within and between layers, consistent with total energy calculations within DFT. However, the configuration with ferromagnetically stacked FM layers is lower in energy than the one with antiferromagnetically stacked FM layers only by ~0.1 meV/Ru. ED calculations, performed on various two-dimensional clusters with different shapes and numbers of sites, confirm the stability of the FM ground state when quantum effects come into play. The addition of the ring-exchange interaction $\mathcal{H}_4^{\text{tot}}$ does not destabilize the FM order, neither for classical nor for quantum spins, but leads to a small tilt of the ordered moment out of the triangular lattice plane (by less than 1° in our model).

After having established the FM character of the ground state, we move on to compute excitations, namely the INS intensity predicted by the magnetic model. We employ linear spin-wave theory (LSWT), complemented by ED to investigate effects beyond LSWT. The results are summarized in Fig. 3, where the ab initio magnetic form factor for Ru^{3+} is taken into account for the calculation of spectral intensities[55], such that the magnetic spectra can be directly compared to neutron scattering experiments.

As previously mentioned, the magnetic moments of the FM ground state of the $\mathcal{H}_2$ Hamiltonian lie within the triangular lattice plane, without picking any preferred direction on the classical level. However, this continuous symmetry is accidental and is lifted by quantum fluctuations, which select the configurations in which the moments are perpendicular to one of the nearest-neighbor bonds[29]. At the *linear* spin wave theory level we then expect the appearance of a gapless pseudo-Goldstone mode, which becomes gapped when quantum effects beyond the lowest order are considered[56,57]. The ED results, compared to the LSWT prediction in Fig. 3b, confirm this picture and find a gap at $\mathbf{q} = 0$ of the order of 1–2 meV.

A further effect beyond LSWT that one might expect here is the appearance of strong scattering continua even in magnetically ordered phases. Such continua were observed in the honeycomb Kitaev material α-$RuCl_3$[58], where they have been traced back in a spin-wave description to originate from significant anharmonic effects due to Γ_1 exchange[46]. However, despite the dominant off-diagonal Γ_1 exchange in the case of $NaRuO_2$ (cf. Table 1), no substantial scattering continuum is found here and the ED spectrum qualitatively follows the sharp modes of LSWT, as shown in a comparison in Fig. 3b. This can be understood as a consequence of the fact that in the present FM state, the pseudo-Goldstone modes remain at the ordering-wave vector $\mathbf{Q} = 0$ (Γ-point), such that a potential decay of single-magnons into a two-magnon continuum via Γ_1-exchange is kinematically not allowed. We note that the inclusion of ring exchange increases the magnon energies by ~2 meV, but does not qualitatively change the main features of the spectrum.

We also compute the powder-averaged INS spectrum that might be relevant for direct comparison of the predicted FM state to experiments[13]. Here, the effect of inter-plane couplings is included, in order to obtain meaningful integration over out-of-plane momenta. The results from LSWT are shown in Fig. 3c and feature the gapless pseudo-Goldstone mode at the smallest momenta, and a less intense gapless mode around 1.2 $Å^{-1}$ arising from the inter-layer FM stacking. Indeed, such a low-energy mode and dominant FM fluctuations (i.e., small $|\mathbf{q}|$-excitations) are also suggested by recent INS powder data at $T = 0.25$ K on $NaRuO_2$[13].

DISCUSSION

In this work, we investigated the magnetic properties of $NaRuO_2$, a layered system of corner-sharing RuO_6 octahedra, which constitutes a prime example of the realization of anisotropic spin couplings, such as the Kitaev interaction, on a triangular lattice structure. By combining two complementary first-principle methods, TEMA and projED, we derived a $j_{\text{eff}} = 1/2$ pseudospin Hamiltonian for $NaRuO_2$, which displays a sizable *antiferromagnetic* Kitaev coupling. This is a direct consequence of the comparatively smaller nearest-neighbor Ru–Ru bond length in $NaRuO_2$, leading to a dominance of direct hopping mechanisms in contrast to other spin-1/2 Kitaev materials to date. The strongest interactions of the model are however a symmetric Γ_1 exchange and an FM J_1 Heisenberg term. The spin Hamiltonian with bilinear interactions possesses a rather robust FM order, oriented parallel to the triangular lattice plane formed by ruthenium ions, also when longer-range intra- and inter-plane exchange interactions are taken into account.

In a recent work[59], the nearest nearest-neighbor spin Hamiltonian for $NaRuO_2$ has been calculated from quantum chemistry methods. While the signs of the nearest-neighbor couplings match with the ones of our model, the Γ_1 term of ref. [59] is smaller than the J_1 exchange strength, contrary to our results. The authors explore the possibility of destabilizing the FM order by an antiferromagnetic third-neighbors exchange, which is in contrast with our first-principle prediction of an FM J_3 coupling.

The parameters of the magnetic Hamiltonian, as obtained by first-principles calculations with the pristine structure of $NaRuO_2$, place this material deep inside an extended FM phase, which cannot be easily destabilized by perturbing the Hamiltonian around the ab initio point. Since the experimentally available results do not show the conventional features of long-range FM order and suggest the possibility of a marginally insulating Mott

state in $NaRuO_2$[13], we explored the effects of higher-order spin interactions, computing four-spin ring exchange couplings from the projED method. However, although the latter turn out to be of a non-negligible size, they seem insufficiently strong to melt the FM order. Nevertheless, the nature of the ring exchange interaction is strongly anisotropic and its consequences warrant further investigation, also in the context of other Kitaev materials.

Furthermore, employing LSWT calculations and ED on finite clusters, we computed the INS spectra for $NaRuO_2$. Comparison of the powder-average neutron scattering intensity with experimental observations shows a similar weight distribution which may signal the presence of underlying ferromagnetism in the system, although no long-range magnetic order was observed in experiments[13,14]. This raises the question of the role of disorder in the material, which may be addressed in future investigations.

METHODS

First-principles calculations

All first principles calculations employ the crystal structure published in ref. [13]. For the calculation of electronic properties we use the full potential local orbital (FPLO)[60] package 18.00-57 and the Generalized Gradient Approximation (GGA)[61] as the exchange-correlation functional. The correlation for the strongly localized Ru 4d electrons are corrected via the GGA + U approximation using the "atomic limit" implementation[62]. All calculations are carried out on a $12 \times 12 \times 12$ k-grid in the primitive unit cell. Relativistic calculations are performed within the GGA + SOC + U functional. The estimates of the t_1–t_3 hoppings discussed in the "Magnetic model" section have been obtained within a non-relativistic GGA calculation.

The electronic properties (band structure, density of states (DOS)) have been cross-checked with the linearized augmented plane-wave basis set as implemented in Wien2k[63] version 19.1, with Ru 4*d* correlation correction included via the SIC method[64,65] with effective Coulomb repulsion $U_{\text{eff}} = 2$ eV.

We also compute the gyromagnetic *g*-tensor from the first principles. For this calculation, we consider a $[RuO_6]^{9-}$ molecule within the quantum chemistry ORCA 5.03 package[66] with the functional TPSSh, basis set def2-TZVP, and complete active space self-consistent field method for the *d* orbitals CASSCF(5,5). A conductor-like polarizable continuum model (C-PCM)[67] is employed with a Gaussian charge scheme, a van der Waals-type cavity, and an infinite dielectric constant.

Constrained random phase approximation

Based on the electronic structure obtained with the Wien2k package v21.1[63] we estimate the electronic two-particle interaction terms in $NaRuO_2$ with the constrained random-phase approximation (cRPA)[68,69], as implemented in the FHI-gap code[70]. The integration of the Brillouin zone is done on an $8 \times 8 \times 8$ grid. The static low-energy limit of the partially screened interaction is projected onto the relevant orbitals, where screening processes in the same window are excluded. The spherical symmetric expressions for *d* electrons in the atomic limit are based on Slater integrals F_k[65] as follows:

$$U_{\text{avg}} = \frac{1}{(2l+1)^2} \sum_{\alpha\beta} U_{\alpha\beta} = F_0 \tag{4}$$

$$J_{\text{avg}} = \frac{7}{5} \frac{1}{2l(l+1)} \sum_{\alpha \neq \beta} J_{\alpha\beta} = \frac{F_2 + F_4}{14}, \tag{5}$$

where α, β are orbital indices and l is the angular momentum quantum number.

As mentioned in the "Results" section, due to a band crossing of the Ru e_g bands with a Na 3*s* band in $NaRuO_2$, there are two sensible ways to select the relevant orbitals considered in the Wannier projection. We denote results based on the five Ru 4*d* orbitals as $(U_{\text{avg}}, J_{\text{avg}})_{4d}$ and results including also the Na 3*s* band as $(U_{\text{avg}}, J_{\text{avg}})_{4d+3s}$. Since both these options lead to very similar results, further calculations in the main text adopt the average of both cRPA results.

DFT-based derivation of the magnetic model

We extract the dominant magnetic Heisenberg couplings via the TEMA[71–73], which is a two-step process. First, we calculate the total energies within DFT (GGA + U) of different magnetic configurations of chosen supercells of $NaRuO_2$. In the second step, we fit the DFT energy of the different magnetic configurations to an effective Heisenberg spin-1/2 Hamiltonian using the method of least squares. The first step is performed in the VASP 5.3 framework[74] using spin-polarized DFT + U, where we apply the Dudarev scheme[75], with effective Coulomb repulsion $U_{\text{eff}} = 3.5$ eV. Here, we consider 14 different magnetic configurations. The calculations are performed within a $3 \times 2 \times 1$ supercell on a $5 \times 8 \times 3$Γ-centered k-grid with an energy cut-off of 540 eV for the plane-wave basis set. The quality of the TEMA for the considered model is discussed in Supplementary Note 5. We have checked that different values of the effective Coulomb repulsion don't significantly affect the ratio between the various exchange couplings.

As a second method, we employ the so-called projED technique[45]. The approach consists of two main steps. First, an effective 4*d* electronic Hamiltonian $\mathcal{H}_{\text{tot}} = \mathcal{H}_{\text{hop}} + \mathcal{H}_{\text{U}}$ is constructed, where $\mathcal{H}_{\text{hop}}$ consists of complex electronic hopping parameters, determined from first principles via Wannier projection of a relativistic band structure calculation (GGA + SOC). Here, we extract the Wannier functions by using the FPLO[60] package 18.00-57. $\mathcal{H}_{\text{U}}$ contains the electronic two-particle Coulomb interaction[45]. In a second step, the electronic Hamiltonian is solved by ED on a two-site five-orbital cluster and its low energy states are projected onto spin operators, arriving at the desired effective spin Hamiltonian, e.g., $\mathcal{H}_2 = \mathbb{P}\mathcal{H}_{\text{tot}}\mathbb{P} = \sum_{i<j}\sum_{\mu\nu} \mathbb{J}_{i,j}^{\mu\nu} S_i^{\mu} S_j^{\nu}$. Note that here $\mathbf{S}$ is a pseudospin with $j_{\text{eff}} = 1/2$. We employ the projED method for the calculation of nearest-neighbor couplings, while for longer-range interactions we resort to TEMA results. This choice is motivated by the fact that, within projED, the indirect hoppings over multiple sites, which are expected to become more and more important for longer-range couplings, cannot be accounted for due to computational limitations.

We also employ the projED method to extract the four-spin ring exchange Hamiltonian $\mathcal{H}_4^{\text{tot}}$. Due to computational limitations, the parameters are extracted by diagonalizing a four-site three-orbital electronic Hamiltonian involving only Ru t_{2g} orbitals. We adopt this approximation since the aim of this work is to estimate the general form and order of magnitude of the ring exchange interaction in a strongly spin-orbit coupled system like $NaRuO_2$. Possible refinements of this approach are beyond the scope of this work and will be pursued in future studies.

Iterative minimization (classical spins)

We obtain the classical ground state of the spin Hamiltonian $\mathcal{H}$ by performing a numerical minimization of the energy on a finite lattice with periodic boundary conditions. We employ an *iterative method* in which the orientation of the spins (unit vectors at the classical level) is initialized with random values and updated by performing local moves. A single update is performed by selecting a random site *i* and changing its spin orientation according to

$$\mathbf{S}_i \mapsto -\frac{\mathbf{h}_i}{\|\mathbf{h}_i\|} \quad \text{where} \quad \mathbf{h}_i = \left(\frac{\partial \mathcal{H}}{\partial S_i^x}, \frac{\partial \mathcal{H}}{\partial S_i^y}, \frac{\partial \mathcal{H}}{\partial S_i^z}\right). \tag{6}$$

In other words, we anti-align the spin at site *i* to the effective field $\mathbf{h}_i$ created by the interactions with the other spins in the lattice. The

procedure is repeated several times until the minimum energy is reached. To try to mitigate the possibility of ending up in local energy minima, we perform a number of different calculations starting from different random initializations. Most numerical results have been obtained on a triangular lattice of $N = 12 \times 12 = 144$ sites. For calculations involving inter-layer couplings, we used a three-dimensional cluster of $N = 6 \times 6 \times 6 = 216$ sites.

Exact diagonalization

We perform ED of the $j_{\text{eff}} = 1/2$ model on two-dimensional clusters of up to $N = 27$ sites. The INS intensity at momentum $\mathbf{q}$ and energy ω is given by

$$\mathcal{I}(\mathbf{q},\omega) \propto f^2(\mathbf{q}) \int \mathrm{d}t\, e^{-i\omega t} \sum_{\mu,\nu} \left(\delta_{\mu,\nu} - \frac{k_\mu k_\nu}{k^2}\right) \left\langle S^\mu_{-\mathbf{k}}(t) S^\nu_{\mathbf{k}}(0)\right\rangle \qquad (7)$$

where $f(\mathbf{q})$ is the atomic form factor of Ru^{3+}. To compute it, we employ the continued fraction method[76]. To access a higher number of q-points, we plot together results coming from clusters of different shapes and sizes up to $N = 27$ (clusters shown in Supplementary Note 3), similar to as done in, e.g., ref. [46]. On all clusters and in the LSWT results, the intensity at small momenta $\mathbf{q} \approx 0$ is found so large that in a simple color plot, the intensity at $\mathbf{q}$ away from $\mathbf{q} \approx 0$ would be almost invisible. We, therefore, opted for Fig. 3b to plot a smaller broadening and a reduced intensity *only* at the $\mathbf{q} = 0$ point. Without this adjustment, the intensity at $\mathbf{q} = 0$ would appear ~21 times larger, rendering the rest of the dispersion invisible to the eye. q-points with $\mathbf{q} \neq 0$ are broadened by 1 meV Gaussians and $\mathbf{q} = 0$ by 0.5 meV, in order to make the gap in ED better visible by eye.

Linear spin-wave theory

LSWT calculations are performed with the SpinW 3.0 library[77]. The INS intensity is computed by taking the powder average of Eq. (7).

DATA AVAILABILITY

The datasets generated during the current study are available under the following publicly accessible repository https://gude.uni-frankfurt.de/handle/gude/232 or alternatively from the corresponding authors upon reasonable request.

CODE AVAILABILITY

The custom codes implementing the calculations of this study are available from the authors upon reasonable request.

Received: 22 February 2023; Accepted: 21 June 2023;
Published online: 13 July 2023

REFERENCES

1. Anderson, P. Resonating valence bonds: a new kind of insulator? *Mater. Res. Bull.* **8**, 153–160 (1973).
2. Fazekas, P. & Anderson, P. W. On the ground state properties of the anisotropic triangular antiferromagnet. *Philos. Mag.* **30**, 423–440 (1974).
3. Balents, L. Spin liquids in frustrated magnets. *Nature* **464**, 199–208 (2010).
4. Kitaev, A. Anyons in an exactly solved model and beyond. *Ann. Phys.* **321**, 2–111 (2006).
5. Khaliullin, G., Koshibae, W. & Maekawa, S. Low energy electronic states and triplet pairing in layered cobaltate. *Phys. Rev. Lett.* **93**, 176401 (2004).
6. Khaliullin, G. Orbital order and fluctuations in mott insulators. *Prog. Theor. Phys.* **160**, 155–202 (2005).
7. Jackeli, G. & Khaliullin, G. Mott insulators in the strong spin-orbit coupling limit: from Heisenberg to a quantum compass and Kitaev models. *Phys. Rev. Lett.* **102**, 017205 (2009).
8. Winter, S. M. et al. Models and materials for generalized Kitaev magnetism. *J. Phys. Condens. Matter* **29**, 493002 (2017).
9. Takagi, H., Takayama, T., Jackeli, G., Khaliullin, G. & Nagler, S. E. Concept and realization of Kitaev quantum spin liquids. *Nat. Rev. Phys.* **1**, 264–280 (2019).
10. Trebst, S. & Hickey, C. Kitaev materials. *Phys. Rep.* **950**, 1–37 (2022).
11. Janssen, L. & Vojta, M. Heisenberg–Kitaev physics in magnetic fields. *J. Phys. Condens. Matter* **31**, 423002 (2019).
12. Shikano, M., Delmas, C. & Darriet, J. $NaRuO_2$ and $NaxRuO_2{\cdot}yH_2O$: new oxide and oxyhydrate with two dimensional RuO_2 layers. *Inorganics* **43**, 1214–1216 (2004).
13. Ortiz, B. R. et al. Quantum disordered ground state in the triangular-lattice magnet $NaRuO_2$. *Nat. Phys.* https://doi.org/10.1038/s41567-023-02039-x (2023).
14. Ortiz, B. R., Sarte, P. M., Avidor, A. H. & Wilson, S. D. Defect control in the heisenberg-kitaev candidate material $naruo_2$. *Phys. Rev. Mater.* **6**, 104413 (2022).
15. Liu, W. et al. Rare-earth chalcogenides: a large family of triangular lattice spin liquid candidates*. *Chin. Phys. Lett.* **35**, 117501 (2018).
16. Bordelon, M. M. et al. Field-tunable quantum disordered ground state in the triangular-lattice antiferromagnet $NaYbO_2$. *Nat. Phys.* **15**, 1058–1064 (2019).
17. Baenitz, M. et al. $NaYbS_2$: a planar spin $\frac{1}{2}$ triangular-lattice magnet and putative spin liquid. *Phys. Rev. B* **98**, 220409 (2018).
18. Sarkar, R. et al. Quantum spin liquid ground state in the disorder free triangular lattice $naybs_2$. *Phys. Rev. B* **100**, 241116 (2019).
19. Dai, P.-L. et al. Spinon fermi surface spin liquid in a triangular lattice antiferromagnet $NaYbSe_2$. *Phys. Rev. X* **11**, 021044 (2021).
20. Kimchi, I. & Vishwanath, A. Kitaev-Heisenberg models for iridates on the triangular, hyperkagome, kagome, fcc, and pyrochlore lattices. *Phys. Rev. B* **89**, 014414 (2014).
21. Jackeli, G. & Avella, A. Quantum order by disorder in the Kitaev model on a triangular lattice. *Phys. Rev. B* **92**, 184416 (2015).
22. Rousochatzakis, I., Rössler, U. K., van den Brink, J. & Daghofer, M. Kitaev anisotropy induces mesoscopic $\mathbb{Z}_2$ vortex crystals in frustrated hexagonal antiferromagnets. *Phys. Rev. B* **93**, 104417 (2016).
23. Becker, M., Hermanns, M., Bauer, B., Garst, M. & Trebst, S. Spin-orbit physics of $j = \frac{1}{2}$ mott insulators on the triangular lattice. *Phys. Rev. B* **91**, 155135 (2015).
24. Li, K., Yu, S.-L. & Li, J.-X. Global phase diagram, possible chiral spin liquid, and topological superconductivity in the triangular Kitaev-Heisenberg model. *N. J. Phys.* **17**, 043032 (2015).
25. Shinjo, K., Sota, S., Yunoki, S., Totsuka, K. & Tohyama, T. Density-matrix renormalization group study of Kitaev-Heisenberg model on a triangular lattice. *J. Phys. Soc. Jpn* **85**, 114710 (2016).
26. Wang, S. et al. Comprehensive study of the global phase diagram of the *J*-*K*-Γ model on a triangular lattice. *Phys. Rev. B* **103**, 054410 (2021).
27. Dey, T. et al. Spin-liquid behavior in $J_{\text{eff}} = \frac{1}{2}$ triangular lattice compound Ba_3Ir-Ti_2O_9. *Phys. Rev. B* **86**, 140405 (2012).
28. Catuneanu, A., Rau, J. G., Kim, H.-S. & Kee, H.-Y. Magnetic orders proximal to the Kitaev limit in frustrated triangular systems: application to $Ba_3IrTi_2O_9$. *Phys. Rev. B* **92**, 165108 (2015).
29. Maksimov, P. A., Zhu, Z., White, S. R. & Chernyshev, A. L. Anisotropic-exchange magnets on a triangular lattice: spin waves, accidental degeneracies, and dual spin liquids. *Phys. Rev. X* **9**, 021017 (2019).
30. Stavropoulos, P. P., Pereira, D. & Kee, H.-Y. Microscopic mechanism for a higher-spin Kitaev model. *Phys. Rev. Lett.* **123**, 037203 (2019).
31. Amoroso, D., Barone, P. & Picozzi, S. Spontaneous skyrmionic lattice from anisotropic symmetric exchange in a Ni-halide monolayer. *Nat. Commun.* **11**, 5784 (2020).
32. Riedl, K. et al. Microscopic origin of magnetism in monolayer 3*d* transition metal dihalides. *Phys. Rev. B* **106**, 035156 (2022).
33. Riedl, K., Gati, E. & Valentí, R. Ingredients for generalized models of κ-phase organic charge-transfer salts: a review. *Crystals* **12** (2022).
34. Thouless, D. J. Exchange in solid 3he and the Heisenberg Hamiltonian. *Proc. Phys. Soc.* **86**, 893 (1965).
35. Riedl, K. et al. Spin vortex crystal order in organic triangular lattice compound. *Phys. Rev. Lett.* **127**, 147204 (2021).
36. Holt, M., Powell, B. J. & Merino, J. Spin-liquid phase due to competing classical orders in the semiclassical theory of the Heisenberg model with ring exchange on an anisotropic triangular lattice. *Phys. Rev. B* **89**, 174415 (2014).
37. Misguich, G., Lhuillier, C., Bernu, B. & Waldtmann, C. Spin-liquid phase of the multiple-spin exchange Hamiltonian on the triangular lattice. *Phys. Rev. B* **60**, 1064–1074 (1999).
38. Block, M. S. et al. Exotic gapless mott insulators of bosons on multileg ladders. *Phys. Rev. Lett.* **106**, 046402 (2011).
39. Motrunich, O. I. Variational study of triangular lattice spin-1/2 model with ring exchanges and spin liquid state in $\kappa - (ET)_2cu_2(CN)_3$. *Phys. Rev. B* **72**, 045105 (2005).
40. Cookmeyer, T., Motruk, J. & Moore, J. E. Four-spin terms and the origin of the chiral spin liquid in mott insulators on the triangular lattice. *Phys. Rev. Lett.* **127**, 087201 (2021).
41. Li, Y. et al. Ring-exchange interaction effects on magnons in Dirac magnet $CoTiO_3$. Preprint at *arXiv* https://doi.org/10.48550/arXiv.2212.05278 (2022).
42. Kim, B. J. et al. Novel $J_{\text{eff}} = 1/2$ mott state induced by relativistic spin-orbit coupling in Sr_2IrO_4. *Phys. Rev. Lett.* **101**, 076402 (2008).

43. Johnson, R. D. et al. Monoclinic crystal structure of $\alpha - RuCl_3$ and the zigzag antiferromagnetic ground state. *Phys. Rev. B* **92**, 235119 (2015).
44. Chaloupka, J. C. V. & Khaliullin, G. Magnetic anisotropy in the kitaev model systems Na_2IrO_3 and $RuCl_3$. *Phys. Rev. B* **94**, 064435 (2016).
45. Riedl, K., Li, Y., Valentí, R. & Winter, S. M. Ab initio approaches for low-energy spin Hamiltonians. *Phys. Status Solidi B* **256**, 1800684 (2019).
46. Winter, S. M. et al. Breakdown of magnons in a strongly spin-orbital coupled magnet. *Nat. Commun.* **8**, 1–8 (2017).
47. Winter, S. M., Li, Y., Jeschke, H. O. & Valentí, R. Challenges in design of Kitaev materials: magnetic interactions from competing energy scales. *Phys. Rev. B* **93**, 214431 (2016).
48. Wolf, B. et al. Combined experimental and theoretical study of hydrostatic he-gas pressure effects in α-rucl$_3$. *Phys. Rev. B* **106**, 134432 (2022).
49. Kaib, D. A. S. et al. Electronic and magnetic properties of the RuX_3 (X=Cl, Br, I) family: two siblings—and a cousin? *npj Quantum Mater.* **7**, 75 (2022).
50. Rau, J. G., Lee, E. K.-H. & Kee, H.-Y. Generic spin model for the honeycomb iridates beyond the Kitaev limit. *Phys. Rev. Lett.* **112**, 077204 (2014).
51. Zhang, Q. & Li, T. Bosonic resonating valence bond theory of the possible chiral spin-liquid state in the triangular-lattice Hubbard model. *Phys. Rev. B* **104**, 075103 (2021).
52. Riedl, K., Valentí, R. & Winter, S. M. Critical spin liquid versus valence-bond glass in a triangular-lattice organic antiferromagnet. *Nat. Commun.* **10**, 2561 (2019).
53. Walker, L. R. & Walstedt, R. E. Computer model of metallic spin-glasses. *Phys. Rev. B* **22**, 3816–3842 (1980).
54. Sklan, S. R. & Henley, C. L. Nonplanar ground states of frustrated antiferromagnets on an octahedral lattice. *Phys. Rev. B* **88**, 024407 (2013).
55. Do, S.-H. et al. Majorana fermions in the Kitaev quantum spin system α-rucl3. *Nat. Phys.* **13**, 1079–1084 (2017).
56. Rau, J. G., McClarty, P. A. & Moessner, R. Pseudo-goldstone gaps and order-by-quantum disorder in frustrated magnets. *Phys. Rev. Lett.* **121**, 237201 (2018).
57. Elliot, M. et al. Order-by-disorder from bond-dependent exchange and intensity signature of nodal quasiparticles in a honeycomb cobaltate. *Nat. Commun.* **12**, 3936 (2021).
58. Banerjee, A. et al. Neutron scattering in the proximate quantum spin liquid α-$RuCl_3$. *Science* **356**, 1055–1059 (2017).
59. Bhattacharyya, P., Bogdanov, N. A., Nishimoto, S., Wilson, S. D. & Hozoi, L. Antiferromagnetic anisotropic exchange competing with Heisenberg nearest-neighbor ferromagnetism in triangular-lattice $NaRuO_2$. Preprint at *arXiv* https://doi.org/10.48550/arXiv.2212.09365 (2022).
60. Koepernik, K. & Eschrig, H. Full-potential nonorthogonal local-orbital minimum-basis band-structure scheme. *Phys. Rev. B* **59**, 1743–1757 (1999).
61. Perdew, J. P., Burke, K. & Ernzerhof, M. Generalized gradient approximation made simple. *Phys. Rev. Lett.* **78**, 1396–1396 (1997).
62. Ylvisaker, E. R., Pickett, W. E. & Koepernik, K. Anisotropy and magnetism in the LSDA + U method. *Phys. Rev. B* **79**, 035103 (2009).
63. Blaha, P. et al. WIEN2k: an augmented plane wave plus local orbitals program for calculating crystal properties (Techn. Universitat, 2019).
64. Anisimov, V. I., Solovyev, I. V., Korotin, M. A., Czyżyk, M. T. & Sawatzky, G. A. Density-functional theory and nio photoemission spectra. *Phys. Rev. B* **48**, 16929–16934 (1993).
65. Liechtenstein, A. I., Anisimov, V. I. & Zaanen, J. Density-functional theory and strong interactions: orbital ordering in mott-hubbard insulators. *Phys. Rev. B* **52**, R5467–R5470 (1995).
66. Neese, F. The ORCA program system. *Wiley Interdiscip. Rev. Comput. Mol. Sci.* **2**, 73–78 (2012).
67. Barone, V. & Cossi, M. Quantum calculation of molecular energies and energy gradients in solution by a conductor solvent model. *J. Chem. Phys. A* **102**, 1995 (1998).
68. Aryasetiawan, F. et al. Frequency-dependent local interactions and low-energy effective models from electronic structure calculations. *Phys. Rev. B* **70**, 195104 (2004).
69. Aryasetiawan, F., Karlsson, K., Jepsen, O. & Schönberger, U. Calculations of Hubbard *U* from first-principles. *Phys. Rev. B* **74**, 125106 (2006).
70. Jiang, H. et al. FHI-gap: A GW code based on the all-electron augmented plane wave method. *Comput. Phys. Commun.* **184**, 348 (2012).
71. Glasbrenner, J. K. et al. Effect of magnetic frustration on nematicity and superconductivity in iron chalcogenides. *Nat. Phys.* **11**, 953–958 (2015).
72. Iqbal, Y. et al. Signatures of a gearwheel quantum spin liquid in a spin-$\frac{1}{2}$ pyrochlore molybdate Heisenberg antiferromagnet. *Phys. Rev. Mater.* **1**, 071201 (2017).
73. Guterding, D., Valentí, R. & Jeschke, H. O. Reduction of magnetic interlayer coupling in barlowite through isoelectronic substitution. *Phys. Rev. B* **94**, 125136 (2016).
74. Kresse, G. & Hafner, J. Ab initio molecular dynamics for liquid metals. *Phys. Rev. B* **47**, 558–561 (1993).
75. Dudarev, S. L., Botton, G. A., Savrasov, S. Y., Humphreys, C. J. & Sutton, A. P. Electron-energy-loss spectra and the structural stability of nickel oxide: an LSDA+U study. *Phys. Rev. B* **57**, 1505–1509 (1998).
76. Dagotto, E. Correlated electrons in high-temperature superconductors. *Rev. Mod. Phys.* **66**, 763 (1994).
77. Toth, S. & Lake, B. Linear spin wave theory for single-*Q* incommensurate magnetic structures. *J. Phys. Condens. Matter* **27**, 166002 (2015).

ACKNOWLEDGEMENTS

We thank V. Krewald and I.I. Mazin for valuable advice regarding the ab initio calculations. We thank also D. Ceresoli, M. Imada, J. Kuneš, and P.A. Maksimov for fruitful comments and discussions. R.V., A.R., K.R., D.A.S.K., and F.F. gratefully acknowledge support by the Deutsche Forschungsgemeinschaft (DFG, German Research Foundation) for funding through Project No. 411289067 (VA117/15-1), TRR 288—422213477 (project A05) and CRC 1487—443703006 (project A01). L.B. was supported by the DOE, Office of Science, Basic Energy Sciences under Award No. DE-FG02-08ER46524. S.D.W. acknowledges support by DOE, Office of Science, Basic Energy Sciences under Award No. DE-SC0017752.

AUTHOR CONTRIBUTIONS

R.V., S.D.W., and L.B. conceived the project. Density functional theory calculations were performed by A.R., K.R., cRPA calculations by S.B., projED calculations by K.R., and calculations on magnetic models by D.A.S.K. and F.F. All authors contributed to the writing of the paper.

FUNDING

Open Access funding enabled and organized by Projekt DEAL.

COMPETING INTERESTS

The authors declare no competing interests.

ADDITIONAL INFORMATION

Supplementary information The online version contains supplementary material available at https://doi.org/10.1038/s41535-023-00567-6.

Correspondence and requests for materials should be addressed to Aleksandar Razpopov, David A. S. Kaib or Roser Valentí.